Numerical modelling of extension in the faulted crust: effects of localised and regional deformation on basin stratigraphy

ter Voorde, M.; Cloetingh, S.A.P.L.

published in
Geological Society Special Publication
1995

document version
Publisher's PDF, also known as Version of record

Numerical modelling of extension in faulted crust: effects of localized and regional deformation on basin stratigraphy

M. TER VOORDE & S. CLOETINGH
Institute of Earth Sciences, Vrije Universiteit, De Boelelaan 1085, 1081 HV Amsterdam, The Netherlands

Abstract: A numerical model for localized and regional deformation during crustal extension is presented. In this model, the behaviour of the faulted upper crust is coupled with ductile deformation in the lower crust and upper mantle. The incorporation of finite extension rates makes the model an appropriate tool for analysing the effects of synrift processes on the basin structure and stratigraphy.

Modelling results indicate that the shape of a basin depends not only on the fault geometry and the deformation mechanism, but also on the behaviour of the lower lithosphere. The authors demonstrate that onlap and offlap patterns can be caused by successive activation of a series of faults.

As shown by the modelling, the amount of footwall uplift of the fault blocks is determined by the integrated effects of deep-lithospheric and near-surface processes. Of particular importance are the spacing of the faults, the amount of extension, the depth of necking, the depth of the Moho, and the lithospheric rigidity. The rate of extension turns out to be a very important but undervalued factor for the postrift to synrift sediment thickness ratio. It is shown that this ratio increases with the extension velocity.

Following the introduction of the simple uniform stretching model for the development and evolution of rifted sedimentary basins (McKenzie 1978), substantial progress has been made in the refinement and expansion of this concept. Regional instead of local isostatic compensation has been included (Beaumont *et.al.* 1982), thermal calculations have been sophisticated (Stephenson 1989; Burrus & Audebert 1990), and models including faults have been introduced (Kusznir *et al.*, 1987; Waltham 1989). The application of these models has mainly focused on predictions for paleobathymetry, heat-flow and subsidence (e.g. Issler & Beaumont 1985; Kooi *et al.* 1992), and regional scale stratigraphy modelling (e.g. Janssen *et al.* 1993; Reemst *et al.* 1994).

The fundamental importance of major basement faulting is shown by many deep seismic reflection profiles. Half grabens, linked together in various ways, form the building blocks of the architecture of rifts. This is illustrated in Fig. 1, giving an example of a horst-like feature observed in Lake Tanganyika in the east African rift zone (Fig. 1a, after Scott & Rosendahl 1989) and an example of a number of half grabens with similar polarity, forming the Potiguar Basin in the Northeast Brazilian rift system (Fig. 1b, after de Matos 1992). Like most rifted basins, these structures are developed by 'pulsed' extension. Movement occurs along one fault system for some period of time, and then shifts to another, often adjacent, fault system. Though there is often an overlap in the periods of activation of different faults, basins rarely, if ever, develop by simultaneous subsidence of all the fault blocks. However, to our knowledge, no quantitative models exist predicting basin evolution by alternating activation of different faults. In this paper, a numerical model for crustal extension is presented, including deformation along faults, and allowing for different periods of activation for every separate fault.

As shown by various authors, active extensional faulting and sedimentation are intimately linked (White *et al.* 1986; Barr 1987; Underhill 1991; Prosser 1993; Steel 1993). Underhill (1991) demonstrated that depositional sequences recognized in the Inner Morray Firth basin are controlled by regional subsidence associated with local extensional fault activity. Prosser (1993) showed that in settings tectonically active during sediment deposition, the synrift and postrift stratigraphy depends on the rate of faulting and basin formation. Not only the accommodation space for sediments is controlled by fault activity, but also the sediment supply: an uplifted footwall in a region with tilted fault blocks mostly erodes, and its erosion products accumulate in the most adjacent basins.

Features of synrift stratigraphy that might be explained by tectonic mechanisms, are for example, (i) the existence of unconformities, (ii) the different

From Buchanan, P. G. & Nieuwland, D. A. (eds), 1996, *Modern Developments in Structural Interpretation, Validation and Modelling*, Geological Society Special Publication No. 99, pp. 283–296.

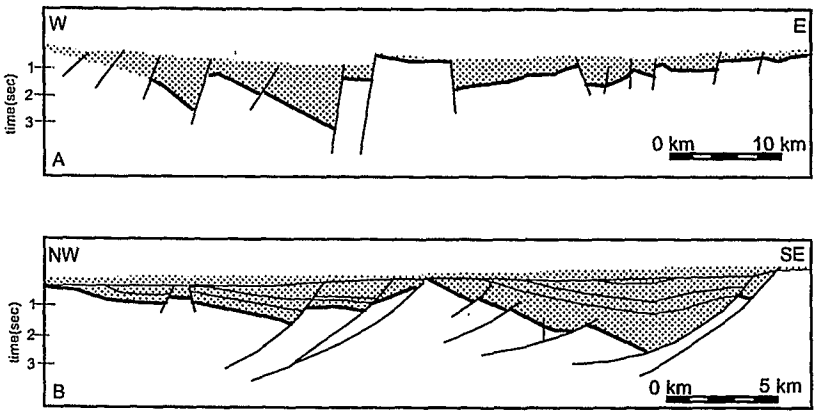

Fig. 1. (a) Schematic profile across Lake Tanganyika in the East African rift system. (After Scott & Rosendahl, 1989.) (b) Interpreted cross section across the onshore Portguar basin in the northeast Brazilian rift system. (After de Matos 1992.)

amounts of footwall uplift in tilted fault block regions, and (iii) the variation in the ratio between synrift and postrift subsidence.

(i) Onlap and offlap patterns observed in stratigraphic sequences have been explained by various mechanisms, including glacio-eustatic sealevel changes (Vail *et al.* 1977) and temporal fluctuations in the intraplate stress field, changing the flexural shape of the basin (Cloetingh 1986). By incorporating faults and a finite duration of the synrift phase in numerical models for lithospheric deformation, some additive tectonic mechanisms can be studied, especially for local, small scale (third order) patterns.

(ii) The amount of footwall uplift of a fault block depends on the size of the block (i.e. the spacing of the faults) and the amount of rifting (Yielding 1990). If we start from the notion that footwall uplift is caused by the integrated effect of faulting and flexural compensation (e.g. Kusznir *et al.* 1991), the amount of footwall uplift should be determined not only by the characteristics of faulting, but also by the properties of the lithosphere. These are for example the lithospheric rigidity, the depth of the Moho and the depth around which the lithospheric thinning occurs.

(iii) The pure shear model of McKenzie (1978) predicts that the ratio of the synrift to postrift sediment thickness is constant for given crustal and lithosphere thickness. Kusznir & Ziegler (1992) developed a more sophisticated model including faults, and concluded that the synrift to postrift sediment thickness ratio is controlled by the location (and thus spacing) of the faults and their individual amounts of displacement. In both these studies an instantaneous stretching phase was assumed. In this paper the importance of the velocity of extension as a third and critical parameter controlling the synrift to postrift ratio will be demonstrated.

To study the topics mentioned above a new numerical model was developed, combining brittle tectonics at shallow levels with ductile deep lithosphere behaviour, and incorporating a finite duration of the synrift phase. This offers the opportunity to quantify the influence of time on various processes acting during and after extensional basin formation. Furthermore, the model can be utilized to predict the interaction between faulting at the near surface and pure shear deformation in the deeper lithosphere.

Lithosphere rheology

The model assumes that the lithosphere deforms by localized deformation in the upper crust, and by diffuse deformation in the lower lithosphere (Fig. 2). This is in accordance with observations from deep seismic sections (e.g. Marsden *et al.* 1990; Bois 1993) and can be explained by the rheological profile of the continental lithosphere (Fig. 3a), showing a relatively strong, mostly brittle upper crust, underlain by a ductile, mostly weak lower crust. This rheological stratification has implications not only for the deformation mechanism (normal faulting in the upper crust versus diffuse deformation in the lower lithosphere), but also for the flexural response of the lithosphere to loading. This response, as will be shown later, is largely dependent on the so-called 'depth of necking', defined as the level which, in the absence of isostatic forces, would remain horizontal during extension (Braun & Beaumont 1989; Weissel & Karner 1989; Kooi *et al.* 1992).

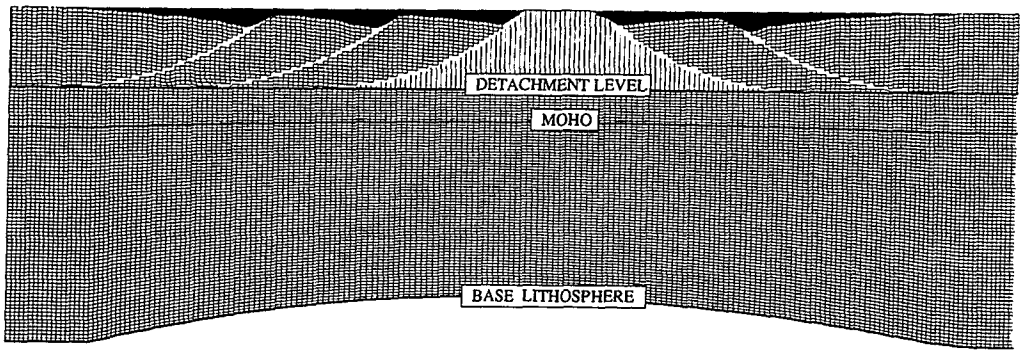

Fig. 2. Model configuration. The upper part extends by deformation along faults, the lower part by a diffuse, sinusoidal thinning of which the location and wavelength can be varied.

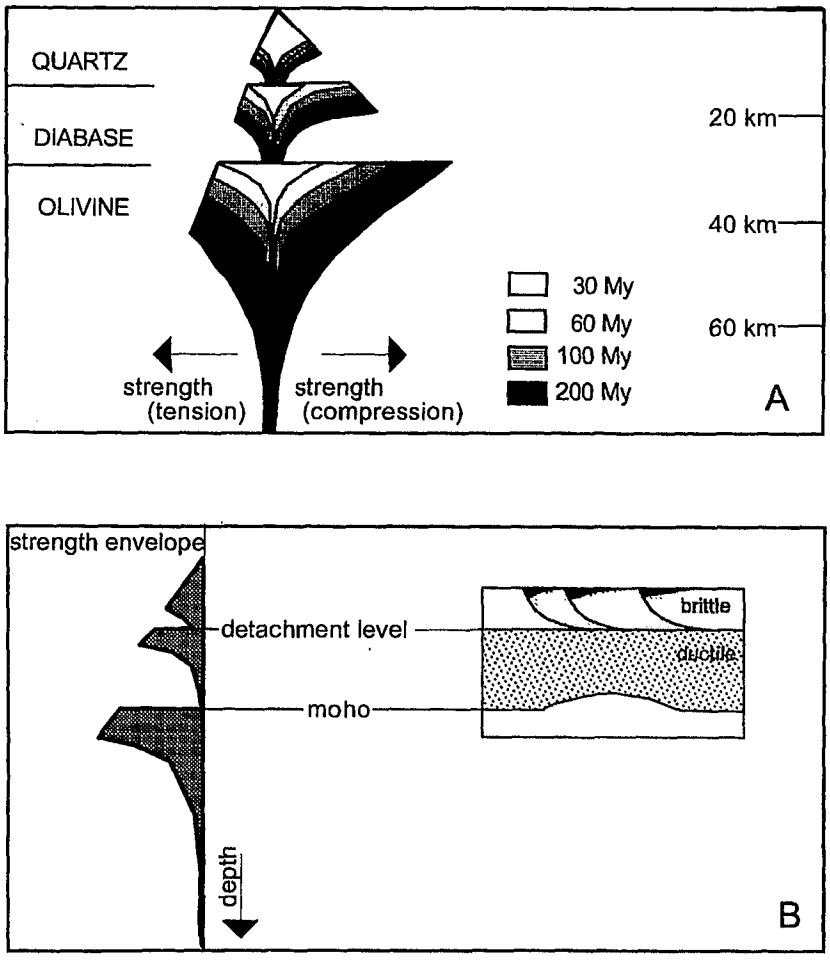

Fig. 3. (**a**) Strength profiles for a number of thermal ages and adapting a ductile strain-rate of 10^{-15} s^{-1} for a stratified continental lithosphere (after Beekman 1994). (**b**) In the model, the necking level and the detachment zone where the faults flatten out, are assumed to coincide, and are located in the lower, weak part of the upper crust.

Finite-element modelling of extension in the lithosphere (e.g. Bassi *et al.* 1993), shows that the lithosphere necks around the level of maximum strength. However, the necking depth as estimated from forward basin modelling shows large variations for different case studies (see Cloetingh *et al.* in press). The values vary from 25 km in the Tyrrhenian Sea (Spadini *et al.* 1995) to 7 km in the Pannonian Basin (Van Balen & Cloetingh 1994) and often do not coincide with the position of the strong layers in the lithosphere. This can be explained in different ways. If more than one strong layer is present in the lithopshere, the 'effective' level of necking will be positioned between these layers. A multi-layer, temperature-dependent rheology, with strong layers in the upper crust and upper mantle, can thus be cast in terms of a level of necking at lower crustal levels – which are the levels in which major faults sole out (Van Balen & Cloetingh 1994; Van der Beek *et al.* 1994). Alternatively, as a result of the crust being detached from the strong upper mantle, intracrustal necking can be the preferred mechanism (Van der Beek *et al.* 1994).

In this model, we assume that the lithosphere thins around the detachment zone in the lower weak part of the upper crust, where the normal faults sole out (Fig. 3b).

Description of the model

The 2D forward model is time dependent and calculates the deformation of the crust and lithosphere during extension. The model geometry consists of a rectangular area of which the upper part extends by localized deformation, i.e. deformation along faults, and the lower part by diffuse deformation (Fig. 2). With this principle, adopted from Kusznir *et al.* (1987), a coupling between the brittle near surface and the ductile lower lithosphere is accomplished.

The total deformation time is divided into small timesteps. In each timestep, the velocity field is calculated on a rectangular grid. A second, moving grid, representing the extending basin, is deformed according to this velocity field. The resulting basin is filled with sediments up to sealevel by defining a new horizontal line in the moving grid after each timestep. The vertical position of this line is equal to the position of the sealevel. Subsequently, at the end of each timestep, the temperature field and the flexural deformation of the basin are calculated.

The deformation in the upper part of the model is calculated according to a method described by Waltham (1989). In this 'brittle' region a fault is defined (Fig. 4). On one side of the model a constant horizontal velocity, the velocity of extension, is imposed. The direction field of the velocity

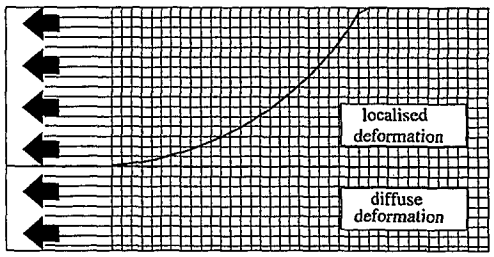

Fig. 4. Principle of the model. In the rectangular area a fault is defined. On one side of the area a constant horizontal velocity is imposed. The velocity in each gridpoint is then calculated from volume conservation.

is prescribed by defining 'isogons', lines along which the movement-direction is constant, and equal to the dip of the fault at the point of intersection (Fig. 5). The magnitude of this velocity field is calculated from the condition of volume conservation

$$\nabla \cdot \vec{v} = 0 \qquad (1)$$

where v is the velocity. This equation is solved using an implicit finite difference technique (Waltham 1989).

The deformation in the ductile lower layer is defined as a sinusoidal varying pure shear thinning, also satisfying the condition of volume conservation. The horizontal location of maximum thinning, l_{max}, can be varied, eventually leading to an asymetric pattern. In this case, the wavelength of thinning is different on both sides of lmax, while the amplitude is the same. Also the width of the region over which the thinning occurs can be varied. As a result, the model is capable of quantifying the effects of a large range of different thinning patterns in the ductile layer.

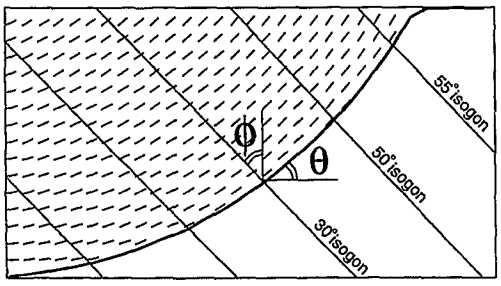

Fig. 5. Isogons are the lines along which the direction of the velocity, Θ, is constant. In this model isogons are straight lines intersecting the fault and dipping ϕ degrees anticlockwise from vertical. Θ is equal to the dip of the fault at the point of intersection. The short lines indicate the velocity directions.

To simulate multiple faults in an area, we simply add the velocity fields resulting from each separate fault. In this way, the interaction between several faults that are activated in specified periods can be modelled. These periods may either coincide, leading to simultaneous activity of the faults, be seperated, yielding successive fault activation, or partly overlap.

The temperature during and after the deformation is calculated from the heat equation

$$\frac{\partial T}{\partial t} = \nabla(\kappa \nabla T) - \vec{v}\nabla T + \frac{F}{\rho C} \quad (2)$$

where

T = temperature (°C)
t = time(s)
κ = thermal diffusivity ($m^2 s^{-1}$)
F = function of heat production ($W m^3$)
ρ = density ($kg m^{-3}$)
C = specific heat ($J kg^{-1} °C^{-1}$)

as described by Ter Voorde & Bertotti (1994). The flexure is calculated by means of the thin plate approximation (Turcotte 1979) given by equation (3):

$$\frac{d^2}{dx^2}\left[D(x)\frac{d^2w}{dx^2}\right] + F\frac{d^2w}{dx^2} + (\rho_a - \rho_s)\, g\, w(x) = q(x) \quad (3)$$

where

w = deflection (m)
D = rigidity (Nm)
F = horizontal force ($N m^{-1}$)
ρ_a = density asthenosphere ($kg m^{-3}$)
ρ_s = density sediments ($kg m^{-3}$)
g = gravitational acceleration ($m s^{-2}$)
q = vertical load ($N m^{-2}$)

The load q is calculated by vertical integration of the density contrast $\Delta\rho$, caused by deformation of the crust, temperature changes and deposited sediments, relative to the undeformed crust:

$$q(x) = \int \Delta(\rho(x, z)\,(1 - \alpha T(x, z))\, g\, dz \quad (4)$$

where

α = thermal expansion coefficient (K^{-1})

Equation (3) is solved using a finite difference method (e.g. Bodine *et al.* 1981).

We assume that after each timestep regional isostatic equilibrium is reached.

During its development, the modelled basin is assumed to be continuously filled with sediments up to sealevel. As a result, if the sealevel is assumed to remain constant, the sedimentation rate is linearly dependent on the rate of extension. As sedimentation patterns are in general dependent on several other parameters, for example sediment supply, topography, the transport medium and the sediment type, this assumption is a strong simplification. However, this modelling approach is capable of isolating the effects of fault tectonics from the effects of other mechanisms.

Effects of normal faulting on basin configuration

Extensional faulting controls the synrift stratigraphy in various ways. Fault configuration and deformation mechanism of the hanging wall have a very straightforward effect on basin shape, whereas the extension rates and time intervals of activation determine the sedimentation patterns in the basin.

The velocity description for hangingwall deformation, as adopted from Waltham (1989), allows any fault shape to be modelled, as long as it flattens out at depth. Figure 6 shows examples for a straight fault, a listric fault and a ramp-flat-ramp fault. As shown, the effect of the different fault geometries on the basin shape is quite pronounced. The requirement that the faults have to flatten out at a certain level is often, but not always, met in natural structures, and thus leads to restrictions on the application of the model. Examples of faults

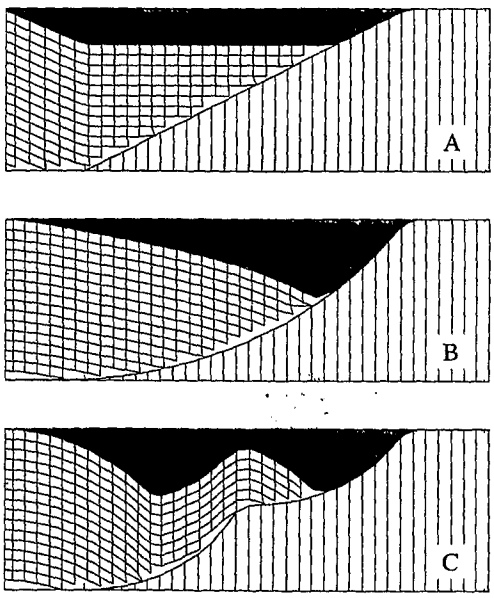

Fig. 6. Crustal deformation resulting from 20% of extension, for different fault geometries. (**a**) Straight fault, (**b**) listric fault, (**c**) ramp-flat-ramp fault. Isogons are assumed to be vertical.

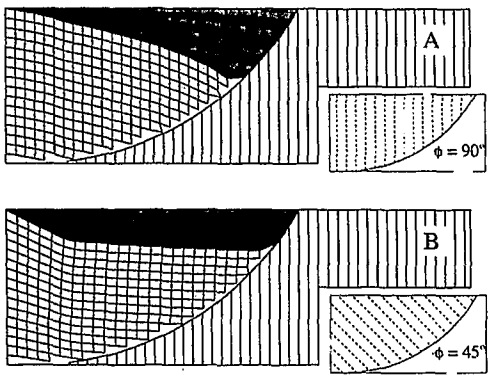

Fig. 7. Crustal deformation due to 20% of extension along a listric fault, for different isogon dips. The isogons are shown on the inset figures. (a) $\phi = 90°$, (b) $\phi = 45°$.

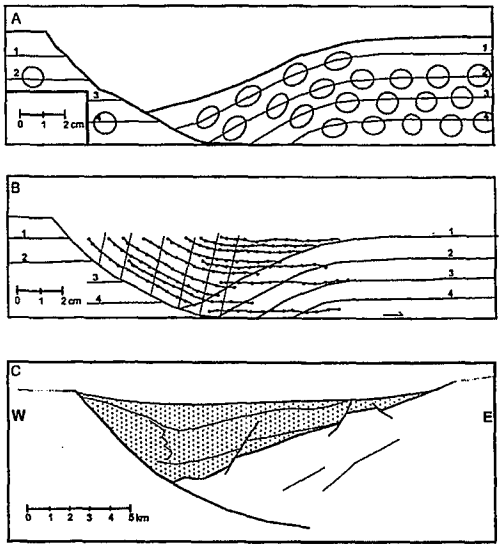

Fig. 8. (a) Result of a clay-model experiment in which the clay hanging wall has been extended 6 cm from the clay-clad aluminium footwall. (After Dula 1991.). (b) Displacement paths of material points, determined from the experiment shown in Fig. 8a. Positions of selected marker points were plotted at 0.5 cm increments of extension. (After Dula 1991.). The result can be explained by inclined simple shear, with a shear angle of 20°. (c) Interpretation of SOHIO Spring Valley seismic line, showing the Schell Creek fault. (After Gans *et al.* 1985). No vertical exaggeration.

flattening out with depth are the Murre Fault, offshore Newfoundland (Tankard & Welsink 1987) and the Corsair fault, offshore Texas (Christiansen 1983).

The deformation characteristics of the hanging wall can be changed in the model by varying the shape and dip of the isogons. This paper is restricted to parallel, non-curved isogons, resulting in hanging wall deformation according to the inclined simple shear mechanism. The influence of the dip of the isogons (thus the shear angle) is shown in Fig. 7, where isogon dips are 90° and 45° respectively. As can be observed in Fig. 7, the deepest point of the basin moves towards the fault with steepening isogons.

Information about deformation mechanisms of faulting can be obtained by dynamical numerical modelling (e.g. Van Wees 1994) and sandbox modelling (e.g. McClay 1989; Dula 1991; Withjack *et al.* 1995). Figures 8a and b show a result from sandbox modelling by Dula (1991). The inclined shear construction (with a shear angle of 20°) produces the best approximation to the observed hanging wall deformation. A natural example is provided by the Schell Creek Range – Spring Valley near the northern Snake Range, east-central Nevada (Fig. 8c, after Gans *et al.* 1985). The Schell Creek fault flattens out at a depth of 10–15 km. A wedge of west-dipping refectors has been observed, indicating synrift sedimentation. Also this basin can be explained by an inclined, almost vertical, shear mechanism.

If not stated otherwise, the isogons will be vertical in all the following modelling results. The other parameters used in the model are summarized in Table 1.

Table 1. *Standard parameters used in the model*

Crustal density	2700 kg m^{-3}
Mantle density	3300 kg m^{-3}
Surface temperature	0°C
Asthenosphere temperature	1330°C
Base lithosphere	125 km
Thermal diffusivity	10^{-6} m^2 s^{-1}
Flexural rigidity	7×10^{20} Nm
Young's modulus	7×10^{10} N m^{-2}
Poisson's ratio	0.25
Thermal expansion coefficient	3.4×10^{-5} $°C^{-1}$
Moho depth	35 km
Necking (detachment) depth	30 km

Normal faulting and synrift stratigraphy

Patterns of onlap and offlap as observed in stratigraphic sequences can be explained by eustatic sealevel changes (Vail *et al.* 1977), large scale changes in the flexural shape of the basin due to intraplate stresses (Cloetingh 1986), and on a more local scale by fault-tectonics.

Hardy (1993) examined the effects of variations

in stretching rates during rifting on the synrift stratigraphy in a domino fault block system, using a diffusion model for erosion and sedimentation, combined with a constant background sedimentation rate. He predicted complex synrift sequences, showing offlap at the fault block crest at increasing stretching rates, and onlap at decreasing stretching rates.

An important advantage of the model presented here above the domino fault block model (Hardy 1993) is that the fault blocks can move sequentially and in different orders, while the domino fault block model assumes that all the dominoes move simultaneously.

Figure 9 demonstrates the effects of extension along three listric faults for two different sequences of fault activation. In case (a) the faults are activated from the left to the right, leading to small scale offlap patterns (indicated by the boxes). In case (b) the faults are activated from the right to the left, resulting in onlap patterns. The condition for the arising of the onlap/offlap patterns is that the spacing between the faults is narrow, so that the half-grabens bounded by the different faults overlap.

An example of case (a) is observed in the Shetland region, north of Scotland (Earle *et al.* 1989). The upper crust of this area consists of half-graben basins formed by extension and subsidence during the Devonian to Carboniferous and Permian to Jurassic periods. The half-graben basins developed above listric faults which dip southeast and sole out into a detachment surface which is a reactivated Caledonian thrust fault.

Figure 10a shows an interpreted seismic section beneath the Hebrides shelf. In each of these basins, sedimentary fill thickens westward, indicating that the faults were active during deposition (Earle *et al.* 1989). The fault activation in this area must have started in the southeast and moved to the northwest, causing the offlap of Permian–Triassic sediments on the Devonian-Carboniferous sediments. In this case, however, some overlap in the time intervals and later rotation and erosion must have occurred. Figure 10b shows the result of a modelling simulation carried out for this scenario (fault activation from the SE to the NW, followed by uplift and erosion).

Apparently, the successive, non-simultaneous activation of a number of faults can provide a new explanation for observed synrift onlap and offlap patterns, provided that the spacing between the faults is narrow, so that the affected areas overlap. To the authors' knowledge, no attention has been given to this mechanism sofar. Especially on seismic sections with poorly imaged faults, this mechanism for the origin of onlap and offlap patterns could easily be overlooked.

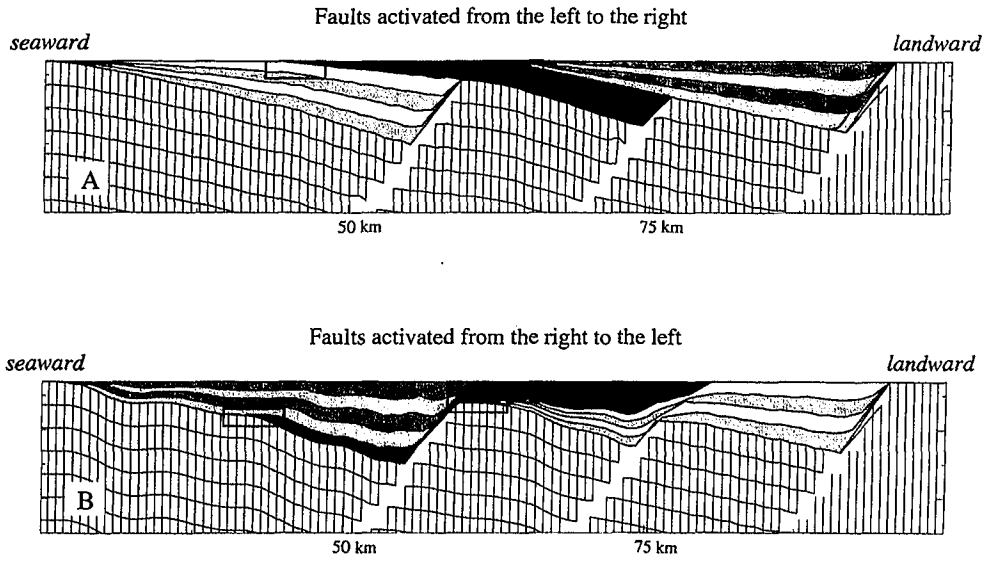

Fig. 9. Crustal deformation due to 12 km of extension along three listric faults, activated successively. (**a**) Faults are activated from the left to the right. Boxes mark offlap patterns. (**b**) Faults are activated from the right to the left. Boxes mark onlap patterns. Small scale undulations are produced numerically, as a result of the deformation of the faults themselves. Vertical exaggeration = 2.8

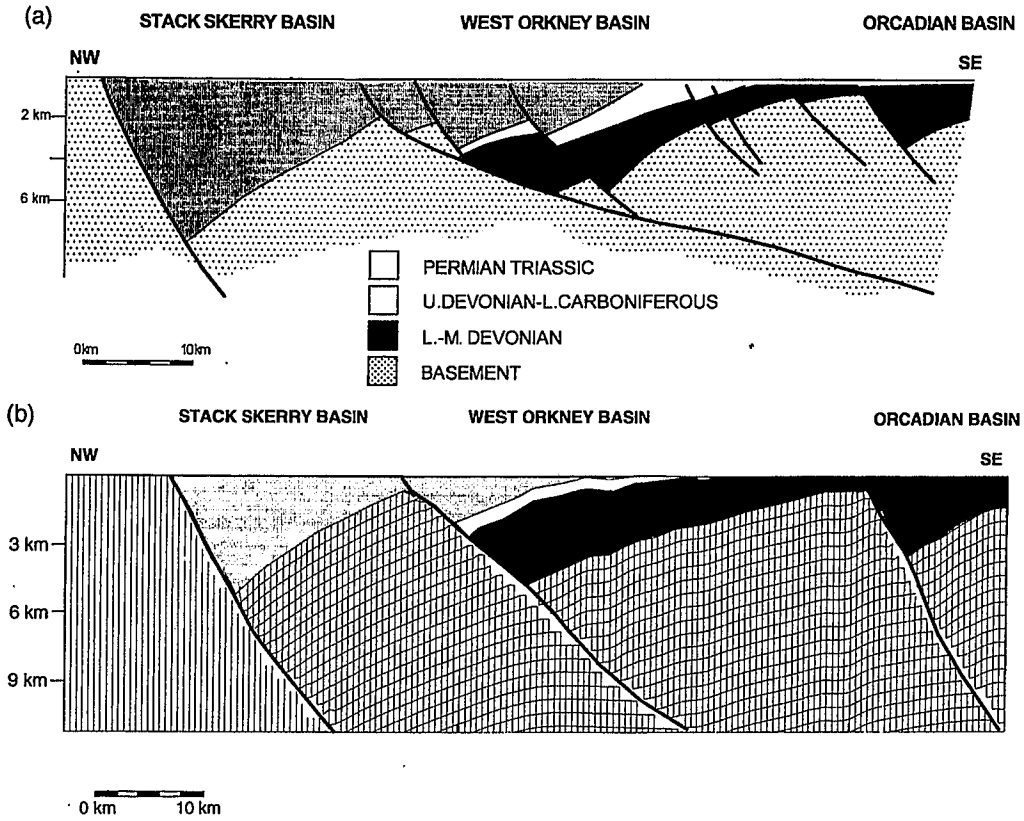

Fig. 10. (a) Geological section across the half grabens beneath the Hebrides Shelf, north of Scotland (after Earle *et al.* 1989). The faults must have been active succesively, from the SE to the NW. (b) Modelling result, obtained by activating the faults succesively, but with some overlap in the time intervals, from the SE to the NW, followed by flexural uplift and erosion.

Footwall uplift and the properties of the lithosphere

The redistribution of loads due to the deformation along faults results in a flexural bending of the lithosphere. As a consequence, the shape of the basin changes. The final shape of a basin is thus an integrated effect of the small scale faulting and the large scale flexural response. The features of this response depend on various lithosphere properties.

The wavelength of the thinning of the lower lithosphere influences the basin shape: thinning over a large area results in a relatively wide and shallow basin, while thinning over a smaller area results in a basin that is deep and narrow. The deformation of the lower lithosphere is thus reflected in the shape of the basin at the crustal surface (see also Kusznir *et al.* 1987).

In case of upward flexural bending, an uplift of the footwall can be generated (Kusznir & Egan 1989). The total amount of footwall uplift is then a summation of the footwall subsidence due to the fault activity, and the uplift caused by the flexural response. This implies that the amount of footwall uplift is not only a function of fault block size and extension (Yielding 1990), but also of lithosphere properties and the position of the fault block.

The overall state of flexure depends on the density of the infilling sediments, the depth of the Moho and the depth of necking during lithospheric extension. As explained before, the depth of necking is the level of zero vertical motion in the absence of isostatic forces, and is assumed here to coincide with the level at which the faults sole out. This level determines the ratio between thinning of the upper crust, where crustal material is replaced by sediments with, in general, low densities, and thinning of the lower lithosphere, where crustal material is replaced by dense mantle material. A deep level of necking thus results in an upward

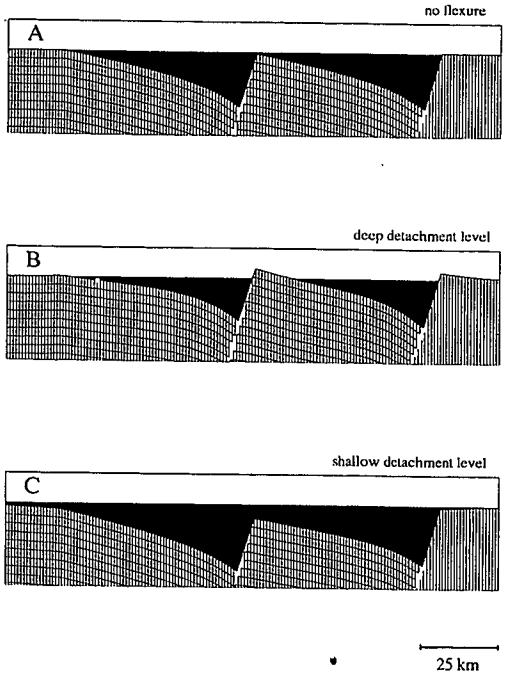

Fig. 11. Lithosphere deformation after 10 km of extension with different values for depth of necking and sediment density. Flexural rigidity is 6×10^{20} Nm, other parameters as in Table 1. (**a**) Zero flexure. (**b**) Flexure included. Detachment depth is 30 km, sediment density is 1.8 g cm^3. (c) Flexure included. Detachment depth is 15 km, sediment density is 2.2 g cm^3. Vertical exaggeration = 3.

state of flexure accompanied by footwall uplift, while a shallow level of necking results in a downward state of flexure (Kooi *et al.* 1992). The different states of flexure are illustrated in Fig. 11, which shows lithospheric deformation after 10 km of extension, for a case without flexure (a), with a necking depth of 30 km and a sediment density of 1.8 g cm^{-3} (b) and with a necking depth of 15 km and a sediment density of 2.2 g cm^{-3} (c). The results displayed in these figures reflect the situation after complete thermal relaxation (i.e. at the end of the postrift phase).

The relation between footwall uplift and necking depth after 10 km of extension along a listric fault is depicted in Fig. 12b. We have adopted the fault configuration of Fig. 12a, with model parameters as given in Table 1. Again, complete thermal relaxation occurred.

As explained above, the amount of footwall uplift increases with the depth of necking. The relationship turns out to be non-linear, the increase in footwall uplift reduces at larger necking depths.

Figure 12c shows the predicted footwall uplift as a function of extension. As can be observed, the amount of footwall uplift increases linearly with the amount of extension. This can easily be understood by considering that equation (3) is a linear equation, and the total load $q(x)$ depends linearly on the amount of extension. This implies that for constant extension rates the footwall uplift is linear with time, if thermal effects are neglected.

The curves describing the relation between footwall uplift and Moho depth (Fig. 12d) are piecewise linear and can be divided into three declining parts. The part with the highest gradient is the part where the Moho depth is less than 20 km. This is the area where the fault-movements occur – an increase in the Moho depth thus means that more crustal instead of mantle material is replaced by the sediments. In the interval between 20 km and 30 km (which is the depth of necking), the position of the Moho is only of limited influence, due to the minor movements here. For a Moho deeper than the necking depth, an increase in Moho depth means that extra crustal material is replaced by mantle material during the thinning, and the gradient increases again.

Figure 12e illustrates the relationship between the amount of footwall uplift and the effective elastic thickness (EET) of the lithosphere. The EET is a measure for the flexural rigidity of the lithosphere, the relation is given in equation (5).

$$D = \frac{E(EET)^3}{12(1-\nu)^2} \tag{5}$$

where

E = Young's modulus (N m^{-2})
ν = Poisson's ratio

Though the amplitude of $w(x)$ decreases with the flexural rigidity, we observe an increase followed by a decrease in the curve describing the footwall uplift. This can be explained by the notion that not only the amplitude changes with the effective elastic thickness, but also the flexural wavelength and the distance at which the flexural response diminishes. Both increase with higher values for rigidity (e.g. Turcotte & Schubert 1982), resulting in a relatively higher footwall uplift.

To conclude, the properties of the lithosphere, such as necking depth, Moho depth and flexural rigidity, exert a strong influence on the amount of footwall uplift.

The synrift to postrift ratio

The subdivision of the subsidence history of an extensional basin into an active rifting phase and a thermal cooling phase is a distinction that cannot be made very strictly in many cases. It was already

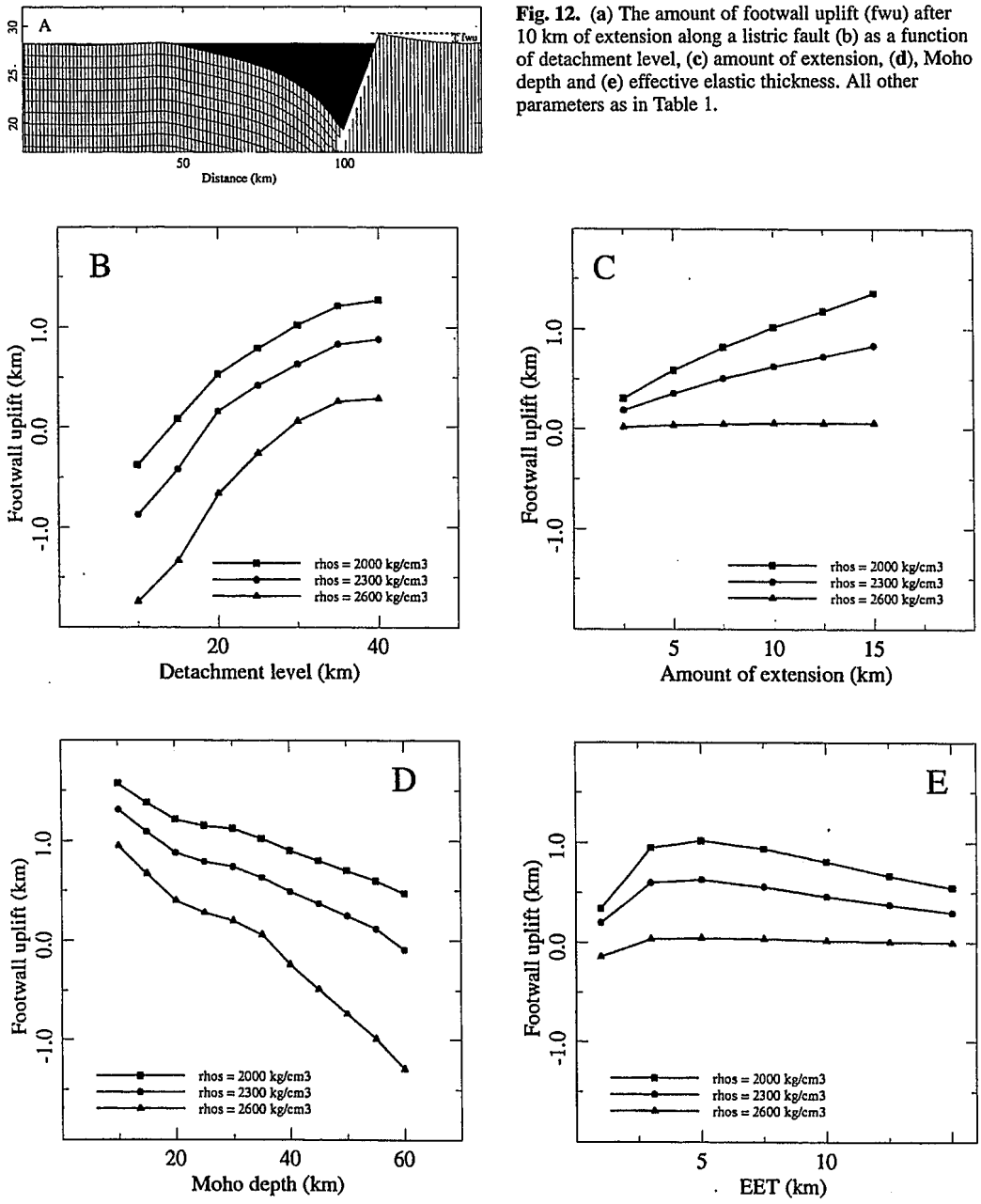

Fig. 12. (a) The amount of footwall uplift (fwu) after 10 km of extension along a listric fault (b) as a function of detachment level, (c) amount of extension, (d), Moho depth and (e) effective elastic thickness. All other parameters as in Table 1.

pointed out by Jarvis & McKenzie (1980) that the finite duration of rifting should be taken into account in subsidence-history calculations if the rifting time is larger than $60/\beta^2$ Ma if $\beta \leq 2$, or $60(1 - 1/\beta)^2$ Ma if $\beta \geq 2$ (where β is the extension factor). Their statement was based on analytical calculations. Ter Voorde & Bertotti (1994) and Bertotti & ter Voorde (1994) found, from a numerical modelling study, that at low extension rates the largest part of the temperature re-equilibration occurs already during rifting instead of during the postrift phase. Therefore, we propose that the ratio of synrift to postrift subsidence is mainly dependent on the rate of stretching.

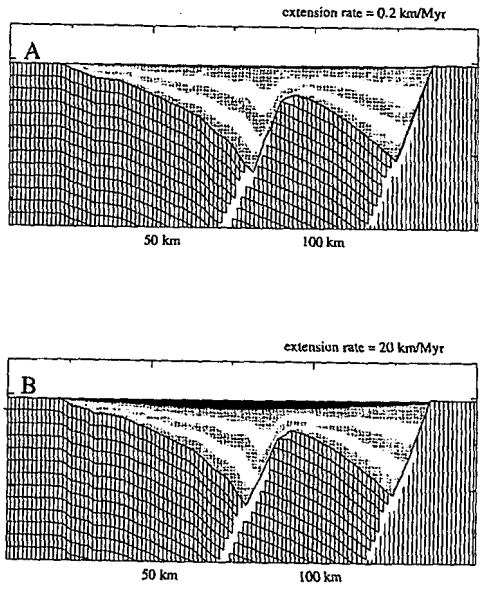

Fig. 13. Lithosphere deformation after 20 km of extension with different extension rates. In light-grey: synrift sediments; in black: postrift sediments. (a) Extension rate is 0.2 km Ma^{-1}, (b) extension rate is 20 km Ma^{-1}. Sediment density is 2600 kg m^{-3}, other model parameters as in Table 1. Small scale undulations are produced numerically, as a result of the deformation of the faults themselves. Vertical exaggeration = 2.8.

Figures 13a and b show modelling results for 20 km of extension along two listric faults, occurring over a period of 10 Ma and 100 Ma respectively. The results indicate that the synrift sediment thickness becomes larger with decreasing extension rates at the expense of the postrift thickness, which is a consequence of the thermal relaxation during extension. In case (a), where the extension rate is 20 km Ma^{-1}, the maximum postrift thickness is 0.9 km, while in case (b), where the extension rate is 0.2 km Ma^{-1}, the maximum postrift sediment thickness is only 0.23 km. Note that the total (synrift + postrift) sediment thickness is equal for both cases. We applied a sediment density of 2600 kg m^{-3}, other parameters as in Table 1.

Figure 14a shows the calculated maximum amplitude with time, for different extension rates. Fault configuration as in Fig. 13. The corresponding β-value is 1.13. The following patterns can be observed:

(i) The amount of flexural uplift during the synrift phase is not linear with time, but shows a decreasing gradient because of the cooling that already takes place during rifting. The total amount of flexural uplift at the end of the synrift phase is lower for cases with lower extension rates.

(ii) If the synrift phase is terminated, only the thermal subsidence remains, decreasing exponentially with time.

(iii) Lithospheric cooling occurs slower at low deformation rates than at high deformation rates, because of the lower temperature gradients that arise in the synrift phase. After 200 Ma, the modelled cases with extension rates higher than 0.40 km Ma^{-1} hardly subside anymore, while the slowest case (0.125 km Ma^{-1}) will still subside some 60 m more.

(iv) The maximum postrift thickness is given by the difference between the amplitude immediately after the synrift phase and the amplitude at the end

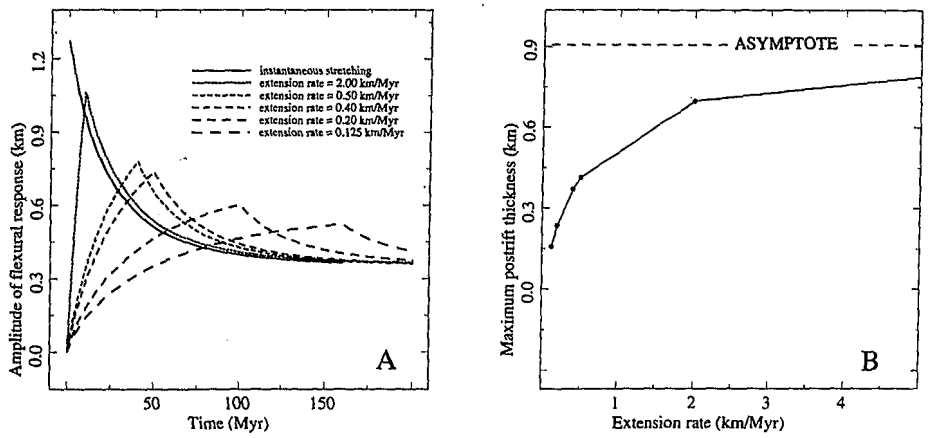

Fig. 14. (a) The maximum flexural uplift of the lithosphere as a function of time for various extension rates. Fault configuration as in Fig. 13, sediment density 2600 kg m^{-3}, other parameters as in Table 1. (b) The maximum postrift thickness of sediments as a function of extension rate. Fault configuration as in Fig. 13. The asymptote gives the maximumpostrift thickness for the case of instantaneous stretching (i.e. infinite extension rate).

of the thermal subsidence. The amplitude at the end of thermal subsidence is not dependent on the extension rate, whereas the amplitude immediately after the synrift phase increases with the extension rate towards an asymptotic value. As a consequence, as shown in Fig. 14b, the maximum postrift thickness also increases with the extension rate.

The conclusion, therefore, is that the extension rate has a substantial influence on the synrift/postrift ratio of sediment thicknesses: for the same amount of total extension, high stretching rates cause thicker postrift sediment piles. This effect becomes even stronger if the sedimentation rate is constant instead of dependent on the extension rate, like in this model. In that case, upon fast extension, subsidence will outpace sedimentation, causing a relatively thinner synrift and thicker postrift sedimentary package.

Conclusions

From the modelling results the following conclusions can be drawn.

(i) A strong coupling exists between small scale tectonics and the synrift stratigraphy in extensional basins. The fault configuration and deformation mechanism have a direct effect on basin shape, and the order of fault activation is a controlling factor for onlap/offlap patterns in stratigraphic sequences, which are commonly interpreted in terms of eustatic sealevel changes.

(ii) To evaluate the structural evolution of an extensional basin, it is necessary to couple the small scale deformation along faults at the near surface with the large scale diffuse deformation in the deeper lithosphere. The wavelength of thinning of the ductile deep lithosphere is reflected directly in the basin shape, while the amount of flexural uplift or subsidence is affected by the depth of necking, the depth of the Moho and the flexural rigidity. These are, apart from the spacing of the faults and the amount of extension, the key factors that determine the amount of footwall uplift. The amount of footwall uplift increases with necking depth, decreases with Moho depth, and shows an increase followed by a decrease with the effective elastic thickness.

(iii) The rate of extension turns out to be a very important factor for the evolution of a rifted basin. The ratio of synrift to postrift sedimentary thickness is largely dependent on stretching rates. For the same amount of extension, the postrift sediment thickness increases exponentially with the stretching rate, whereas the total sediment thickness remains constant.

The authors wish to thank Giovanni Bertotti for many useful suggestions and discussions. Comments of Ronald van Balen and reviews of Lidia Lonergan and an anonymous reviewer are appreciated, and improved the paper substantially. Dick Nieuwland is thanked for comments, and for editorial effort. This research was supported by the IBS (Integrated Basin Studies) project, part of the Joule II research programme funded by the Commission of European Communities (contract No. JOU2-CT 92-0110). Publication No. 950301 of the Netherlands School of Sedimentary Geology.

References

BARR, D. 1987. Structural/stratigraphic models for extensional basins of half-graben type. *Journal of Structural Geology*, **9**, 491–500.

BASSI, G., KEEN, C. E. & POTTER, P. 1993. Contrasting styles of rifting: Models and examples from the eastern Canadian margin. *Tectonics*, **12**, 639–655.

BEAUMONT, C., KEEN, C. E. & BOUTILLIER, R. 1982. On the evolution of rifted continental margins: Comparison of models and observations for the Nova Scotia margin, *Geophysical Journal of the Royal Astronomical Society*, **70**, 667–715.

BEEKMAN, F. 1994. *Tectonic modelling of thick-skinned compressional intraplate deformation.* PhD thesis, Vrije Universiteit, Amsterdam.

BERTOTTI, G. & TER VOORDE, M. 1994. Thermal effects of normal faulting during rifted basin formation. 2: The Lugano Normal Fault and the role of pre-existing thermal anomalies. *Tectonophysics*, **240**, 145–157.

BODINE, J. H., STECKLER, M. S. & WATTS, A. B. 1981. Observations of flexure and the rheology of the oceanic lithosphere, *Journal of Geophysical Research*, **86**, 3695–3707.

BOIS, C. 1993. Initiation and evolution of the Oligo-Miocene rift basins of southwestern Europe: contibution of deep seismic reflection profiling. *Tectonophysics*, **226**, 217–226.

BRAUN, J. & BEAUMONT, C. 1989. A physical explanation of the relation between flank uplifts and the breakup unconformity at rifted continental margins. *Geology*, **17**, 760–764.

BURRUS, J. & AUDEBERT, F. 1990. Thermal and compaction processes in a young rifted basin containing evaporites: Gulf of Lions, France. *American Association of Petroleum Geologists Bulletin*, **74**, 1420–1440.

CHRISTIANSEN, A. F. 1983. An example of a major syn-depositional listric fault. *In*: BALLY, A. W. (ed.) *Seismic Expression of Structural Styles*: American Association of Petroleum Geologists Studies in Geology, **15**, 2.3.1–36-40.

CLOETINGH, S. 1986. Intraplate stress: a new tectonic mechanism for fluctuations in relative sealevel. *Geology*, **14**, 617–620.

——, VAN WEES, J. D., VAN DER BEEK, P.A. & SPADINI, G. Role of pre-rift rheology in kinematics of extensional basin formation: constraints from thermomechanical models of Mediterranean and intracratonic basins. *Marine and Petroleum Geology*, Special IBS Volume, in press.

DULA, W. F. 1991. Geometric models of listric normal faults and rollover folds. *American Association of Petroleum Geologists Bulletin*, **75**, **10**, 1609–1625.

EARLE, M. M., JANKOWSKI, E. J. & VANN, I. R., 1989. Structural and stratigraphic evolution of the Faeroe-Shetland Channel and Northern Rockall Trough. *In*: TANKARD, A. J. & BALKWILL, H. R. (eds) *Extensional Tectonics of the North Atlantic Margins*. American Association of Petroleum Geologists Memoirs, **46**, 461–469.

GANS, P. B., MILLER, E. L., MCCARTHY, J. & OULDCOTT, M .L. 1985. Tertiary extensional faulting and evolving ductile-brittle transition zones in the northern Snake Range and vicinity: New insights from seismic data. *Geology*, **13**, 189–193.

HARDY, S. 1993. Numerical modelling of the response to variable stretching rate of a domino fault block system. *Marine and Petroleum Geology*, **10**, 145–152.

ISSLER, D. R. & BEAUMONT, C. 1985. A finite element model of the subsidence and thermal evolution of extensional basins: Application to the Labrador Continental Margin. *In*: NAESER, N. D. & MCCULLOH, T. H. (eds) *Thermal history of sedimentary basins, methods and case histories*. Springer-Verlag, New York, 239–267.

JANSSEN, M.E., TORNÉ, M., CLOETINGH, S. & BANDA, E. 1993. Pliocene uplift of the eastern Iberian margin: Inferences from quantitative modelling of the Valencia Trough. *Earth and Planetary Science Letters*, **119**, 585-597.

JARVIS, G. T. & MCKENZIE, D. P. 1980. Sedimentary basin formation with finite extension rates. *Earth and Planetary Science Letters*, **48**, 42–52.

KOOI, H., CLOETINGH, S. & BURRUS, J. 1992. Lithospheric necking and regional isostasy at extensional basins. 1. Subsidence and gravity modelling with an application to the Gulf of Lions Margin (SE France). *Journal of Geophysical Research*, **97** (**B12**), 17553–17571.

KUSZNIR, N. J. & EGAN, S. S. 1989. Simple-shear and Pure-shear models of extensional sedimentary basin formation: application to the Jeanne d'Arc Basin, Grand Banks of Newfoundland. *In*: TANKARD, A. J. & BALKWILL, H. R. (eds) *Extensional Tectonics of the North Atlantic Margins*. American Association of Petroleum Geologists Memoir **46**, 305–322.

—— & ZIEGLER, P. 1992. The mechanics of continental extension and sedimentary basin formation: A simple shear/pure-shear flexural cantilever model. *Tectonophysics*, **215**, 117–131.

——, KARNER, G. D. & EGAN, S. 1987. Geometric, thermal and isostatic consequences of detachments in continental lithosphere extension and basin formation. *In:* BEAUMONT, C. & TANKARD, A. J. (eds) *Sedimentary Basins and Basin-Forming Mechanisms*, Canadian Society of Petroleum Geologists Memoir, **12**, 185–203.

——, MARSDEN, G. & EGAN, S. S. 1991. A flexural-cantilever simple-shear/pure-shear model of continental lithosphere extension: applications to the Jeanne d'Arc Basin, Grand Banks and Viking Graben, North sea. *In*: ROBERTS, A. M., YIELDING, G. & Freeman, B. (eds) *The Geometry of Normal Faults*. Geological Society, London, Special Publications, **56**, 41–60.

MARSDEN, G., YIELDING, G., ROBERTS, A. M. & KUSZNIR, N. J. 1990. Application of the flexural cantilever simple-shear/pure-shear model of continental lithosphere extension to the formation of the North Sea basin. *In*: BLUNDELL, D. J. & GIBBS, A. D. (eds) *Tectonic Evolution of the North Sea Rifts*. Oxford University Press, 236–257.

MATOS, R. M. D. DE, 1992. The Northeast Brazilian rift system. *Tectonics*, **11**, 766–791.

MCCLAY, K. R. 1989. Physical models of structural styles during extension. *In*: Tankard, A. J. & Balkwill, H. R. (eds) *Extensional Tectonics of the North Atlantic Margins*. American Association of Petroleum Geologists Memoir, **46**, 95–110.

MCKENZIE, D. P. 1978. Some remarks on the development of sedimentary basins. *Earth and Planetary Science Letters*, **40**, 25–31.

PROSSER, S. 1993. Rift-related linked depositional systems and their seismic expression. *In:* WILLIAMS, G. & DOBB, A. (eds) *Tectonics and Seismic Sequence Stratigraphy*. Geological Society, London, Special Publications, **71**, 35–66.

REEMST, P., CLOETINGH, C. & FANAVOLL, S. 1994. Tectono-stratigraphic modelling of Cenozoic uplift and erosion in the SW Barents Sea. *Marine and Petroleum Geology*, **11**, 478–490.

SCOTT, D. L. & ROSENDAHL, B. R. 1989. North Viking Graben: An East African perspective. *The American Association of Petroleum Geologists Bulletin*, **73**, 155–165.

SPADINI, G., CLOETINGH, S. & BERTOTTI, G. 1995. Thermo-mechanical modeling of the Tyrrhenian Sea: lithospheric necking and kinematics of rifting, **14**, 629–644.

STEEL, R. J. 1993. Triassic–Jurassic megasequence stratigraphy in the Northern North Sea: rift to post-rift evolution. *In*: PARKER, J. R. (ed.) *Petroleum Geology of Northwest Europe: Proceedings of the 4th Conference*. Geological Society, London, 299–315.

STEPHENSON, R. 1989. Beyond first-order thermal subsidence models for sedimentary basins? *In*: CROSS, T. A. (ed.) *Quantitative Dynamic Stratigraphy*. Prentice Hall, 113–125.

TANKARD, A. J. & WELSINK, H. J. 1987. Extensional tectonics and stratigraphy of Hibernia oil field, Grand Banks, Newfoundland. *American Association of Petroleum Geologists Bulletin*, **71**, 1210–1232.

TER VOORDE, M. & Bertotti, G. 1994. Thermal effects of normal faulting during rifted basin formation. 1: A finite difference model. *Tectonophysics*, **240**, 133–144.

TURCOTTE, D. L. 1979. Flexure. *In*: SALTZMAN, B. (ed.) *Advances in Geophysics,* Academic Press, Inc., New York, **21**, 51–86.

—— & SCHUBERT, G. 1982. *Geodynamics, applications of continuum physics to geological problems.* L.Wiley and Sons, USA.

UNDERHILL, J. R. 1991. Controls on Late Jurassic seismic sequences, Inner Moray Firth, UK North Sea: a critical test of a key segment of Exxon's original global cycle chart. *Basin Research*, **3**, 79–98.

VAIL, P., MITCHUM, JR., R. M. & THOMPSON, S. 1977. *Global cycles of relative changes of sea level.* The American Association of Petroleum Geologists Memoir, **26**, 83–97.

VAN BALEN, R. & Cloetingh, S. 1994. Tectonic control of the sedimentary record and stress induced fluid flow: constraints from basin modelling. *In*: PARNELL, J. (ed.) *Geofluids: Origin, Migration and Evolution of Fluids in Sedimentary Basins.* Geological Society, London, Special Publications, **78**, 9–26.

VAN DER BEEK, P., CLOETINGH, S. & ANDRIESSEN, P. 1994. Mechanisms of extensional basin formation and vertical motions at rift flanks: Constraints from tectonic modelling and fission-track thermochronology. *Earth and Planetary Science Letters*, **121**, 417–433.

VAN WEES, J. D. 1994. *Tectonic modelling of basin deformation and inversion dynamics: the role of pre-existing faults and continental lithosphere rheology in basin evolution.* PhD Thesis, Vrije Universiteit, Amsterdam.

WALTHAM, D. 1989. Finite difference modelling of hanging wall deformation. *Journal of Structural Geology*, **11**, 433–437.

WEISSEL, J. K. & KARNER, G. D. 1989. Flexural uplift of rift flanks due to mechanical unloading of the lithosphere during extension. *Journal of Geophysical Research*, **94 (B10)**, 13919–13950.

WHITE, N. J., JACKSON, J. A. & MCKENZIE, D. P. 1986. The relationship between the geometry of normal faults and that of the sedimentary layers in their hanging walls. *Journal of Structural Geology*, **.8**, 897–909.

WITHJACK, M. O., ISLAM, Q. T. & LA POINTE, P. R. 1995. Normal faults and their hanging-wall deformation: An experimental study. *American Association of Petroleum Geologists Bulletin*, **79**, 155–165.

YIELDING, G. 1990. Footwall uplift associated with Late Jurassic normal faulting in the northern North sea. *Journal of the Geological Society, London*, **147**, 219–222.